ADVANCED MATERIALS
www.advmat.de

Recent Progress in Electrically Rechargeable Zinc–Air Batteries

Jing Fu, Ruilin Liang, Guihua Liu, Aiping Yu, Zhenyu Bai, Lin Yang, and Zhongwei Chen**

Over the past decade, the surging interest for higher-energy-density, cheaper, and safer battery technology has spurred tremendous research efforts in the development of improved rechargeable zinc–air batteries. Current zinc–air batteries suffer from poor energy efficiency and cycle life, owing mainly to the poor rechargeability of zinc and air electrodes. To achieve high utilization and cyclability in the zinc anode, construction of conductive porous framework through elegant optimization strategies and adaptation of alternate active material are employed. Equally, there is a need to design new and improved bifunctional oxygen catalysts with high activity and stability to increase battery energy efficiency and lifetime. Efforts to engineer catalyst materials to increase the reactivity and/or number of bifunctional active sites are effective for improving air electrode performance. Here, recent key advances in material development for rechargeable zinc–air batteries are described. By improving fundamental understanding of materials properties relevant to the rechargeable zinc and air electrodes, zinc–air batteries will be able to make a significant impact on the future energy storage for electric vehicle application. To conclude, a brief discussion on noteworthy concepts of advanced electrode and electrolyte systems that are beyond the current state-of-the-art zinc–air battery chemistry, is presented.

1. Introduction

More than ever before, there is an urgent demand for cheaper electrochemical energy storage system with higher energy density to support the next generation commercial and renewable energy technologies. Lithium-ion batteries, owing to its high specific energy (250 Wh kg^{-1}_{cell}), have been a spectacular success in the electric vehicle (EV) market and will continue to improve incrementally for years to come. However, concerns on their high cost (250 US$ kW h^{-1}), inherent safety hazards and intercalation-type cathode performance ceiling have driven the need to investigate alternatives that offer the possibility of going beyond the limits of lithium-ion technology.[1,2]

The electrochemical reduction of atmospheric oxygen as an energy source has long been recognized and has engaged tremendous research efforts to develop high-energy, low-cost, and long-lasting rechargeable zinc–air batteries. A typical zinc–air battery comprises of a zinc anode and an oxygen-permeable cathode assembled in a caustic alkaline electrolyte. The selection of readily accessible zinc and atmospheric oxygen provides advantages of being low cost, having a high theoretical specific energy (1218 Wh kg^{-1}) and, in particular, a very promising volumetric energy density of 6136 Wh L^{-1}.[3] From a safety perspective, the zinc–air battery system using aqueous electrolyte is immune to fire hazard. The simplicity in handling and recycling zinc and zinc oxide also adds onto their economic attractiveness.[4] In fact, commercialization of rechargeable zinc–air batteries has already begun; EOS Energy Storage, FluidicEnergy, ZincNyx are companies which offer zinc–air batteries as grid energy storage systems.[5,6] Currently, the lowest price point offered for these systems is around 160–200 US$ kW h^{-1},[5] and they are forecast to fall to 70 US$ kW h^{-1},[2] which is below the commonly accepted cost per unit energy target (150 US$ kW h^{-1}) required for EVs to be economically competitive.[7]

However, comparing to their high performance ceiling and economic potentials, the current capability of zinc–air batteries is far from satisfactory. Their practical energy densities have been limited to 150–180 Wh kg^{-1},[2] which would struggle to support proper functioning of EVs. The inferior electrode reversibility of zinc–air batteries is also a technological challenge that needs to be addressed. Their current life span of 150 cycles is less than a quarter of the commercially available lithium-ion batteries.[2] Furthermore, factors beyond energy density, such as rate capability and energy efficiency must also be considered for EV applications. As such, there are substantial improvements required for zinc–air batteries prior to their employment as primary energy storage system of EV.

Despite the many challenges ahead, the paths toward achieving the performance requirements are well lit. Slow but steady improvements of each system components are

Dr. J. Fu, R. Liang, G. Liu, Prof. A. Yu, Prof. Z. Chen
Department of Chemical Engineering
Waterloo Institute for Nanotechnology
Waterloo Institute for Sustainable Energy
University of Waterloo
200 University Avenue West, Waterloo, ON N2L 3G1, Canada
E-mail: zhwchen@uwaterloo.ca
Prof. Z. Bai, Prof. L. Yang
School of Chemistry and Chemical Engineering
Key Laboratory of Green Chemical Media and Reactions
Ministry of Education
Henan Normal University
Xinxiang 453007, China
E-mail: baizhengyu@htu.edu.cn, baizhengyu2000@163.com
The ORCID identification number(s) for the author(s) of this article can be found under https://doi.org/10.1002/adma.201805230.

DOI: 10.1002/adma.201805230

being achieved by continuous development efforts around the world. Recent analyses on zinc–air batteries have also predicted promising long-term performance targets at practical energy densities of 500 Wh kg^{-1} and 1400 Wh L^{-1}, and cycle life to as long as 500 cycles.[8] It is important to remember that electrochemically rechargeable zinc–air batteries were only realized in recent years by breakthroughs in bifunctional oxygen electrocatalysts performance (for both oxygen reduction and evolution reactions) and techniques for the suppression of zinc dendrites. Patience and continuous research inputs for this newly revitalized technology are required, but successful fulfillment of its potential will definitely revolutionized the technologies and economic viability of EVs and renewable energy.

Since 2010, researches on electrically rechargeable zinc–air batteries (hereafter referred to as rechargeable zinc–air batteries) grew immensely, mainly involving the topics of efficient bifunctional oxygen electrocatalysts/electrodes and achieving high utilization and cyclability on zinc electrodes. In this progress report, we intend to provide comparatively recent progress on improving zinc electrodes and bifunctional oxygen catalyst/electrodes, followed by reviewing recent novel concepts for advancing battery performance.

2. Current Status

The overall discharge/recharge efficiency (i.e., energy efficiency) and long-term cyclability in zinc–air batteries are far inferior to those of state-of-the-art lithium-ion batteries. These issues are mainly related to zinc irreversibility (related to dendrite formations, shape changes, and ZnO passivation) and high catalytic activation for electrochemical oxygen reduction and evolution processes. This subsection provides the current status and progress of the zinc anode and bifunctional oxygen electrodes with the ongoing approaches.

2.1. Zinc Anode Optimization

In the anode end of zinc–air batteries, researchers have been continuing their search for the perfect solution to the issues associated with zinc performance decay/failure in alkaline condition such as dendrite formation, undesired relocation, and zinc oxide passivation (**Figure 1**a). Traditionally, these issues were reduced with heavy metals, carbon, surfactant additives or surface modification.[9–11] Of the more recent development progresses, anode electrode design and morphology engineering targeting proper allocation/redeposition of zinc species have been proven to be highly effective. Specific designs include construction of high-surface-area porous structures (approach 1 in Figure 1b),[12–14] adoption of 3D conductive host materials (approach 2 in Figure 1b),[15,16] and direct physical inhibition/suppression (approach 3 in Figure 1b).[9,17] Ultimately, the goal of these works is to develop an anode with rigid conductive porous network and minimal inactive material that is self-sufficient in confining the dissolved zincate ions, promoting even distribution of Zn/ZnO depositions, and is immune from failure caused by short-circuiting.[12,14]

Jing Fu is a Mitacs Postdoctoral Fellow at the University of Waterloo. She received her Ph.D. (2018) in chemical engineering under the supervision of Prof. Zhongwei Chen at the University of Waterloo. Her research is focused on the development of advanced nanostructured catalysts/electrodes and polymeric electrolytes for rechargeable zinc–air batteries.

Zhengyu Bai is an associate professor in the School of Chemistry and Chemical Engineering at Henan Normal University. She received her Ph.D. in 2010 from Henan Normal University. Her research is focused on new green energy nanomaterials, such as nanostructured electrocatalysts for fuel cell and metal–air batteries.

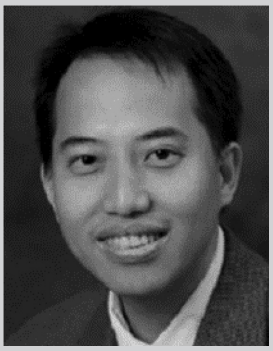

Zhongwei Chen is Canada Research Chair (Tier 1) Professor in Advanced Materials for Clean Energy at University of Waterloo, Fellow of the Canadian Academy of Engineering, Director of Waterloo Center for Electrochemical Energy, and Vice President of International Academy of Electrochemical Energy Science. His research interests are in the development of advanced energy materials and electrodes for fuel cells, metal–air batteries, and lithium-ion batteries.

In one of the earlier attempt demonstrated by Parker et al., porous zinc electrodes were prepared by consecutive argon gas annealing, calcination, and electroreduction of consolidated zinc emulation.[12] The resulting sponge electrodes acquired highly porous structure allowing zinc utilization up to 90% without conductive additive, but it would suffered fast capacity decade within 30 cycles at a relatively low depth of discharge (DOD) of 23%. This electrode design was further improved in following studies by adequate additive and electrolyte selection, allowing it to be cycled at a higher DOD of 40%.[13] The Zn/Ni batteries used to examine the above zinc sponge electrode do suffer significant capacity decays of over 20% at 80 cycles and 50% at 110 to 140 cycles. The authors have attributed the decade to electrolyte dehydration, but the process is likely accelerated

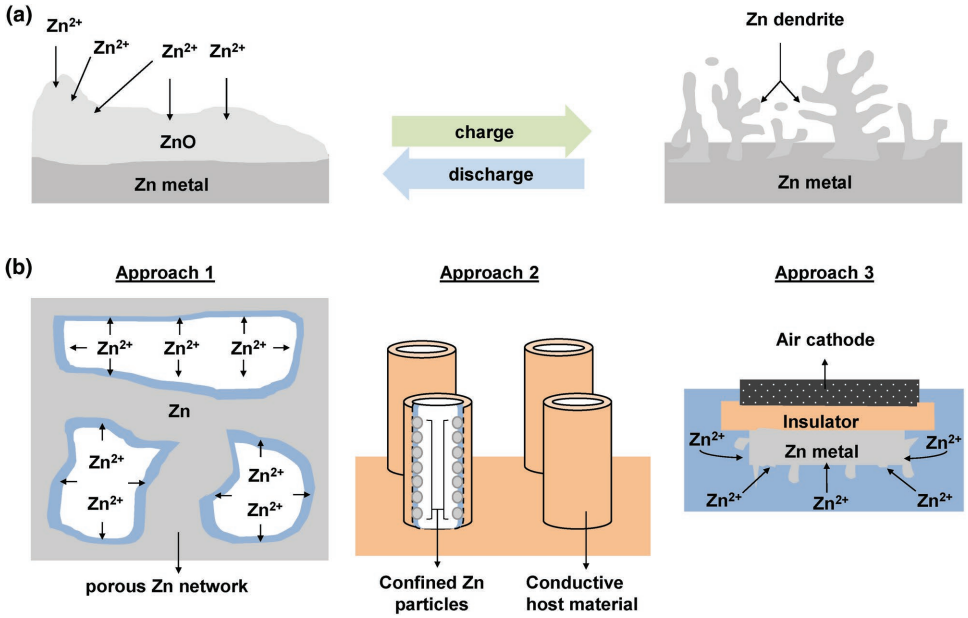

Figure 1. a) Failure mechanism of zinc anodes during cycling. b) Approaches to minimize zinc-dendrite growth and undesired relocation: approach 1, employing a high surface area porous zinc structure; approach 2, confining zinc in 3D conductive host materials; approach 3, direct physical inhibition/suppression.

by eventual collapsed of the porous structure and the increased rate of undesired hydrogen evolution reaction (HER) induced by high surface area of the 3D zinc porous network.[9]

Other zinc electrode designs using electrodeposition or atomic layer deposition of Zn/ZnO on conductive host material such as lithium intercalated TiO_2 nanotube arrays, copper foam, and carbon cloth have also been reported.[15] In these designs, the deposited zinc can be reversibly charge and discharge for over thousands of cycles with high DOD of 80–95%. The even current density distribution established by the 3D conductive host material are the key to the successful dendrite suppression and excellent cyclability displayed in these studies, but they are achieved with low active to host material ratio and consequently low overall energy density. Further optimization in increasing active material loading without performance compensation is required for these designs to be practically meaningful. Smooth zinc deposition can also be achieved by controlling the ion concentration gradient near the electrode surface or tuning the operating current. These favorable conditions were realized by Wang et al. through electrolyte management and pulse charging which lead to improved electrode cycle life.[18] As for physical inhibition of zinc dendrites, Shougo et al. demonstrated a Zn anode backside-plating configuration, in which direct contact of the cathode and the zinc anode is forbidden by a layer of compact insulating polypropylene. This allowed deep cycling of the zinc at 90% DOD for 800 cycles with 88% of the capacity maintained.[17] To compensate for the much improved cyclability though, this configuration sacrificed the shortest path between the two electrodes, leading to higher battery impedance and higher overpotential under operation. The zinc loading in this study is low as well.

On a side note, excellent stability over long periods of cycling (>1000 cycles) have recently been achieved by Zn batteries using mildly acidic or neutral electrolyte.[19,20] The mildly acidic environments inhibit generation of semiconducting ZnO and were examined to facilitate smooth striping/plating of zinc metal for more than 100 cycles without significant overpotential increase.[19] These results may inspire alternate paths toward high zinc cyclability in zinc–air batteries and novel development of acidic/neutral aqueous zinc–air batteries.

2.2. Binfunctional Oxygen Catalyst Engineering

Electrochemical reduction and evolution of oxygen under alkaline conditions are fundamental reactions that allow zinc–air batteries to be electrically rechargeable. Both oxygen reduction (ORR) and evolution (OER) reactions involve four elementary reaction steps, in which ORR proceeds through the formation of HOO* from adsorbed O_2, followed by its further reduction to O* and HO*, while OER proceeds in the reverse direction.[21,22] Unfortunately, these reactions suffer from slow kinetics and thus required an active bifunctional oxygen electrocatalyst to minimize the necessary overpotentials for these reactions. Noble metals (e.g., Pt) or their oxides (e.g., RuO_2, IrO_2) are particularly active for respective ORR or OER electrocatalysis, requiring low overpotentials (e.g., 284 mV on Pt/C for ORR: and 250 mV on RuO_2 for OER at kinetic currents in 0.1 M KOH) to achieve high reaction rates under alkaline conditions.[3,23] However, owing to their scarcity, high cost, limited bifunctionality and stability, their economic competitiveness is relatively low.[24] Over the past decade, researchers have turned to alternative earth-abundant catalyst materials to open up new opportunities in designing low-cost and high-performance bifunctional oxygen catalysts.[25,26] Various types of non-noble metal catalyst materials, such as metal oxides (e.g., cobalt oxides, nickel cobalt oxides, manganese oxides),[27,28] metal chalcogenides (e.g., cobalt sulfides, nickel sulfides),[29] transition-metal-based

molecular complexes (e.g., Co- and Ni–porphyrin complexes,[29] heteroatom-doped carbons (e.g., (N, P)-codoped mesoporous carbon foam,[22,30] and mixtures of these elements have been vigorously studied.[26,31,32] Notable advancements have been made in engineering catalytically active structures of these materials, but there remains much room for improvement.[33] Current strategies for the catalyst design focus on increasing the reactivity and/or number of active sites.[34,35] The active sites in the bifunctional catalysts generally include dual coupled active sites that are effective for respective ORR and OER or a single bifunctional active site that can catalyze the oxygen reaction in both directions. Although the use of decoupled electrocatalysts for separate ORR and OER electrodes was reported to improve the voltage efficiency and cycling stability of the zinc–air battery, this two-electrode configuration is structurally complex and incurs weight and volume penalties of energy and power density.[36] The field of bifunctional oxygen catalysts has seen much progress in recent years,[37] thus this subsection discusses the main roles of engineering material structures and properties in the development of improved bifunctional oxygen catalysts.

2.2.1. Coupling Strategy on Enhanced Bifunctionality

One promising strategy to achieve catalyst bifunctionality is by integrating ORR- and OER-active components into a favorable nanostructure. To this end, a core–corona-structured bifunctional oxygen catalyst consisting of $LaNiO_3$ and nitrogen-doped carbon nanotubes (NCNTs) was explored (**Figure 2**a).[38] In this structure, each NCNT serves as an ORR-active catalyst component anchored on the OER-active $LaNiO_3$ core (Figure 2b). The coupling effect arising from the core–corona structure provides the key to exemplary bifunctional activity of the catalyst compared with state-of-the-art Pt/C and $LaNiO_3$ catalysts. Likewise, nitrogen-doped graphene when chemically coupling with other transition metal oxides such as perovskite (e.g., $La_{0.5}Sr_{0.5}Co_{0.8}Fe_{0.2}O_3$) and spinel (e.g., Co_3O_4) has shown improved catalytic activity for ORR/OER.[39] Although the reaction mechanisms associated with the actual bifunctional active sites in these hybrid catalysts remains unclear, the metal–N bonds derived from synergistic coupling of nanomaterials were found to be the crucial factor for the ORR and OER enhancement.[40] For instance, higher ORR and OER activities were achieved by a Co_3O_4/N-doped graphene hybrid catalyst in comparison to those of Co_3O_4/graphene and Co_3O_4 due to the formation of interfacial Co—N bonds between Co_3O_4 and N-doped graphene.[41] The coupling strategy has also been extended to chemical bonding of WS_2 on carbon nanotubes via tungsten carbide bonding, which provides efficient pathways for transferring electrons by spin polarization to facilitate the ORR/OER catalytic process.[42]

2.2.2. Oxygen Vacancy Enhanced Activity in Metal Oxides

Transition metal oxides with spinel or perovskite crystal structure have been demonstrated as promising bifunctional catalysts for oxygen redox in alkaline solutions.[43] In addition to downsizing and nanostructuring metal oxides to improve mass activity, their catalytic performance can also be significantly enhanced by modifying the surface electronic structure to yield

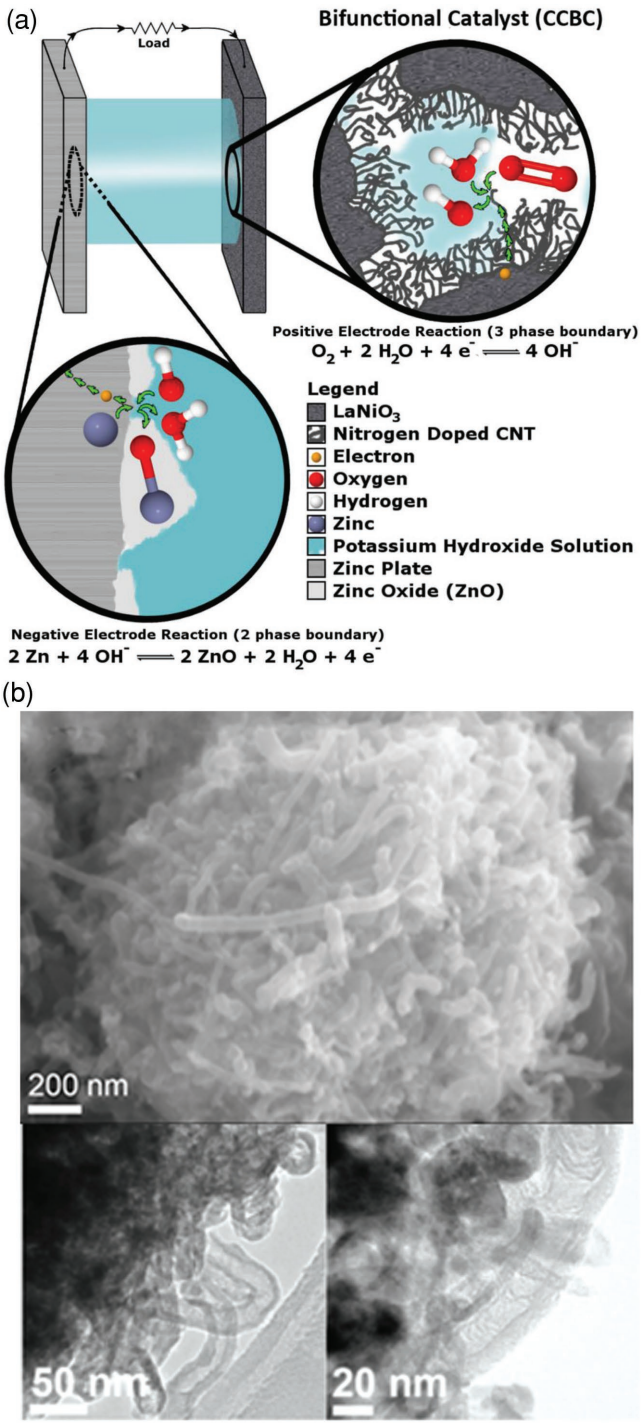

Figure 2. a) Schematic of a zinc–air battery and the redox reactions taking places on the electrodes. The core–corona-structured bifunctional catalyst (CCBC) is applied onto the positive electrode, which catalyzes both the ORR and OER. b) Scanning electron microcopy image and transmission electron microscopy image of the CCBC illustrating the NCNT on the surface of the $LaNiO_3$ core particle. a,b) Reproduced with permission.[38] Copyright 2012, American Chemical Society.

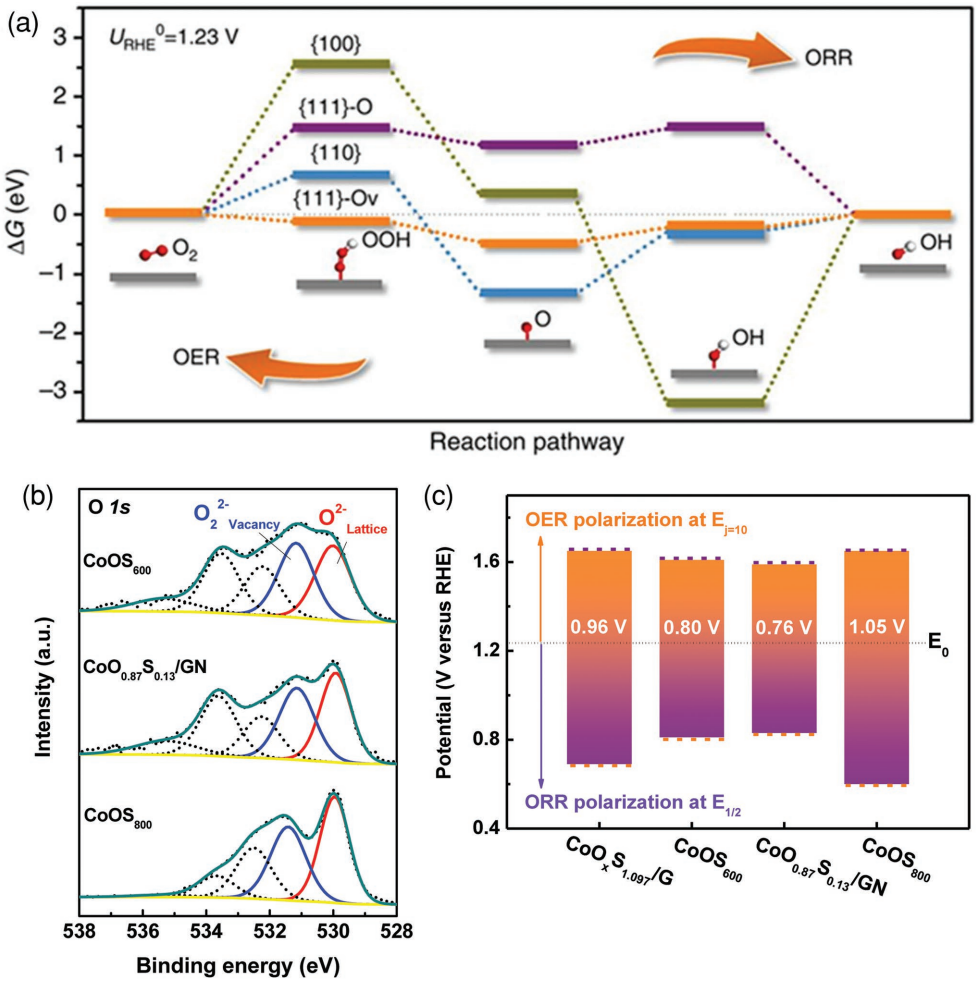

Figure 3. a) The calculated ORR/OER free energy diagram at the equilibrium potential on various facets of pristine CoO and CoO with O-vacancies. Reproduced with permission.[21] Copyright 2016, Springer Nature. b) High-resolution XPS O1s spectra of $CoOS_{600}$, $CoO_{0.87}S_{0.13}$/GN, and $CoOS_{800}$ electrodes. Reproduced with permission.[31] Copyright 2017, Wiley-VCH. c) Potential differences between the $E_{1/2}$ (half-wave potential) of ORR and $E_{j=10}$ of OER (potential at 10 mA cm^{-2}) for all electrodes. Reproduced with permission.[31] Copyright 2017, Wiley-VCH.

high intrinsic activity. Oxygen vacancy has been regarded as an important tool to influence the surface electronic structure and thus catalytic activity[31,44,45] They can be created in the metal oxide crystal lattice by method such as argon plasma treatment and postheat treatment under reducing environment.[44,46] Removal of an oxygen atom from the metal oxide lattice will result in electron (from previously occupied oxygen 2p orbitals) delocalization on metal cations neighboring the vacancy site, which would enhance exposure of active sites and charge transfer to promote catalyst performance.[47] For instance, mesoporous Co_3O_4 nanowires was reduced by $NaBH_4$ treatment leaving oxygen vacancies on the nanowire surface. Relative to pristine Co_3O_4 nanowires, the reduced Co_3O_4 nanowires contain increased portion of OER-active Co^{2+} oxidation state associated with oxygen vacancy formation, resulting in better OER activity due to increased number of active sites and electronic conductivity.[48] Moreover, the capability to control and confine oxygen vacancies on desirable facets will be important to realize the full potential of transition metal oxide as bifunctional catalysts. To this end, 1D single-crystal CoO nanorods (NRs) with desired facets and vacancy defects were explored.[21] The oxygen vacancies present on the oxygen-terminated {111} nanofacets {111}-Ov of CoO NRs are effective for enhancing charge transfer and assuring optimal adsorption energies for intermediates of the ORR and OER, compared with other facets of CoO (**Figure 3**a). As a result, the intrinsic ORR and OER activities of CoO NRs with defect-rich {111}-Ov facets exceeded those of polycrystalline CoO NRs by factors of 7.2 and 2.6, respectively. Besides the formation of oxygen vacancies, filling the oxygen vacancies in defect-rich CoO with sulfur was demonstrated effective for improving the electrocatalytic performance.[31] The amount of oxygen vacancies in the lattice structure was found to increase proportionally with sulfur dopants, in the order of $CoOS_{800}$ < $CoO_{0.87}S_{0.13}$/GN < $CoOS_{600}$ (Figure 3b). Through precisely controlling the sulfur content in cobalt oxysulfides, an optimal oxygen vacancies to lattice oxygen ratio can be obtained for the $CoO_{0.87}S_{0.13}$/GN catalyst to achieve the lowest overpotential toward both ORR and OER among all the electrodes studied, indicative of the highest catalytic bifunctionality (Figure 3c).

2.2.3. Heteroatom Dopants Improved Activity in Carbons and Chalcogenides

The rational doping of heteroatom (e.g., N, S, P, B, and Se) has also emerged as a promising strategy to design carbon-based metal-free bifunctional oxygen catalysts in alkaline media.[49] The introduction of such dopants in carbons can either donate electrons or generate holes to fine-tune electronic properties of adjacent carbon atoms and thus generate catalytic active sites for ORR and OER.[50] By doping carbon with more electronegative heteroatoms such as nitrogen, a net positive charge is created on surrounding carbon atoms, which improves the chemisorption of oxygen and electron transfer, leading to enhanced catalytic activities for ORR/OER.[51] Yang et al. reported the synthesis of 3D architectured, nitrogen-doped graphene nanoribbons (N-GRW) that contain both n-type and p-type nitrogen dopant configurations (**Figure 4**a). It was experimentally found that the quaternary N with n-type doping were responsible for ORR, whereas the pyridinic N with p-type doping in the N-GRW served as active sites for OER. Such conclusions were evident from the formation of quaternary N peak after ORR (due to adsorbed O* and OOH* intermediates on carbon atoms near graphitic N) and increased intensity of pyridinic N peak (due to adsorption of OOH* and O* intermediates on carbon atoms next to the pyridinic N) after OER (Figure 4b). Likewise, doping heteroatoms that are less electronegative (e.g., B) into graphene will create positively polarized active sites for catalytic process.[52] In addition to single atom doping, binary (e.g., N/S, N/B, and N/P) and ternary (e.g., N/B/P and N/F/B) doping of nanostructured carbon catalysts have also been demonstrated to improve catalyst performance,[22,53] which can be attributed to the synergistic electronic interactions between the different dopants and adjacent carbon atoms.[34]

In addition to carbons, transition-metal chalcogenides can be doped with heteroatoms such as P and N, improving their catalytic activity and stability substantially.[29,54–56] Hao et al. introduced N dopants to CoS_2 nanospheres via a hydrothermal reaction.[54] The N doping can have a positive influence on the

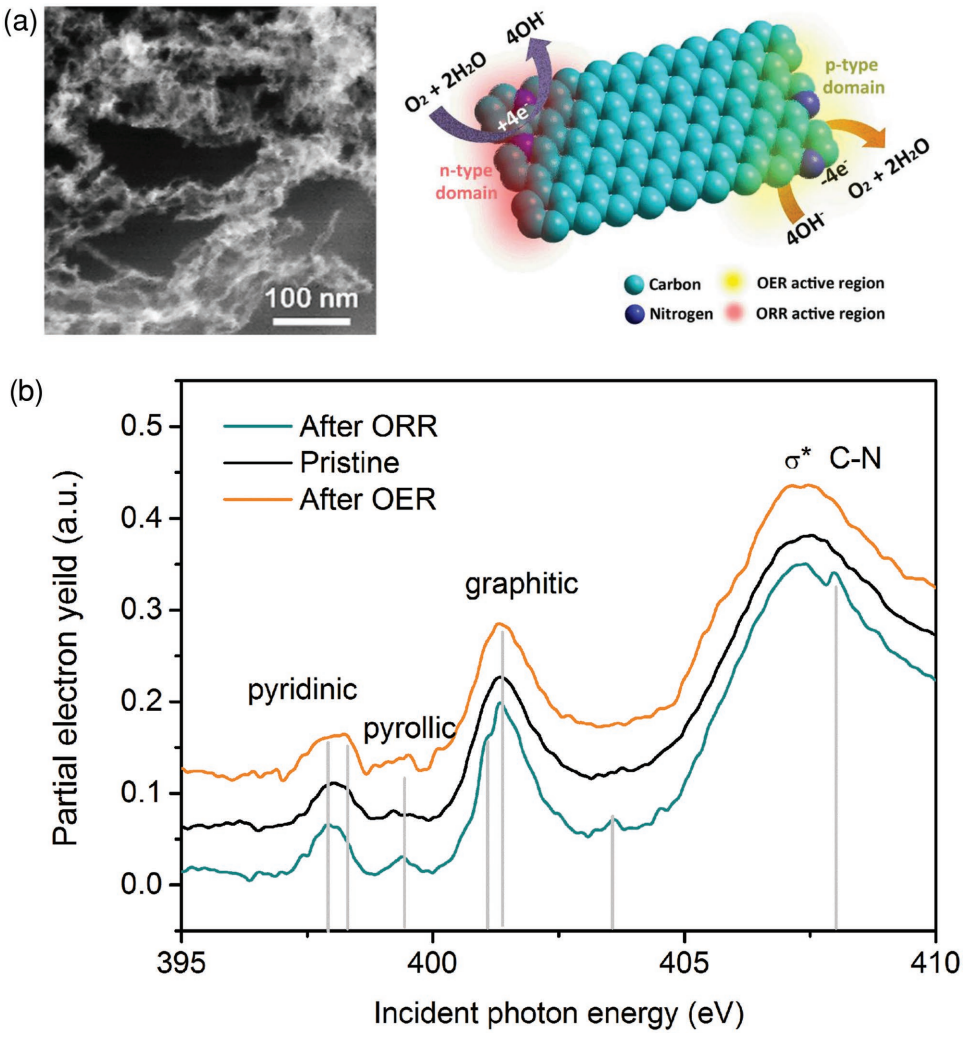

Figure 4. a) High-resolution SEM image and schematic diagram of ORR and OER occurring at different active sites on the n- and p-type domains of the N-GRW catalyst. b) Nitrogen K-edge XANES spectra of N-GRW catalyst, acquired under ultrahigh vacuum, pristine (black line), after ORR (yellow line), and after OER (blue line). a–c) Reproduced with permission.[51a] Copyright 2016, American Association for the Advancement of Science.

electronic density and configurations of CoS_2 nanospheres, which minimize the reaction barriers and thus make the N-enriched CoS_2 nanospheres highly efficient OER catalysts. Guo et al. prepared (N, P)-doped CoS_2 nanoclusters that were embedded inside TiO_2 nanoporous films.[55] The resulting catalyst exhibited improved electrocatalytic ORR/OER activities in an alkaline electrolyte (onset potential of 0.91 V for ORR and 1.41 V for OER vs reversible hydrogen electrode, RHE) that were 50 and 160 mV higher than that of CoS_2 nanoclusters. The improvement was largely due to a decrease in charge transfer resistance of the CoS_2 nanoclusters after doping of N and P.

2.2.4. Rational Construction of Metal–N Active Sites

Transition metal complexes of macrocyclic ligands (e.g., porphyrins and corroles) as bifunctional catalysts for ORR and OER have attracted extensive research interests.[28,29,53c] They possess the ability to stabilize high-valency metal ions in metal–nitrogen coordination structures that are generally believed to be involved as key intermediates in the electrocatalytic ORR and OER processes.[53d] These desirable properties led to the development of Ni^{2+} and Co^{2+} coordinated porphyrin multilayers on a reduced graphene oxide support to expose the Ni-/Co-porphyrin active centers and its subsequent examination in electrocatalytic activity for ORR and OER. The resulting catalyst exhibited low overpotentials for OER (330 mV at 10 mA cm^{-2}_{geo}) and ORR (100 mV at 3.3 mA cm^{-2}_{geo}) in alkaline electrolyte.[29] However, a shortcoming of the porphyrin-based catalysts is their low affinity with the conductive support and thus high tendency to aggregate, resulting in reduced exposure of active sites. In an attempt to alleviate this problem, Co–porphyrin covalent organic frameworks were uniformly coated on carbon nanotube supports through strong intermolecular π–π interactions, as evident from a homogenous distribution of carbon, nitrogen, and cobalt without aggregation (**Figure 5**a). This strategy not only provided uniform Co–porphyrin active sites exposure at the surface but also enabled efficient electron transfer to the conductive support.[57]

In addition to transition metal macrocycle complexes, metal–nitrogen coordination structures can be prepared by pyrolyzing mixtures of nitrogen-containing molecules (e.g., aniline, amino acids, pyrrole) and transition metal ions at high temperatures, leading to the so-called pyrolyzed M-N_x/C catalysts.[58] This concept has spurred the development of various types of metal–organic-framework (MOF)-derived bifunctional catalysts containing Fe- and/or Co–N_x moieties, with different morphologies (e.g., nanocubes, nanocages, nanotues, nanowires, core–shell).[59,60] In these catalysts, MOFs are used as self-sacrificing templates to synthesize metal embedded N-doped carbon matrix through thermal decomposition. This strategy is advantageous due to the homogeneous dispersion of metal–N coordination structures within the conductive and porous carbon matrix, which allows the accommodation of many active sites and promotes charge/mass transfer.[61] However, this strategy still faces difficulties in controlling single-metal-atom-nitrogen configurations in MOFs. Specifically, increasing surface free energy of transition metals during high temperature pyrolysis causes formation of inhomogeneous metal clusters, which can reduce the metal atom efficiency and lead to a relatively weak catalytic activity.[62] To this end, sulfur was introduced to a graphitic carbon nanostructure with combination of nitrogen to generate atomic dispersion of active Fe–porphyrin species (Figure 5b). The resulting single-atom bifunctional catalysts exhibit high catalytic activity toward ORR (obtained half-wave potentials of 0.85 V, ≈20 mV superior to 20% Pt/C) and OER (require small overpotentials of ≈0.39 V at 10 mA cm^{-2}, ≈310 mV superior to 20% Pt/C, Figure 5c).[60]

2.2.5. Corrosion Resistant Supports

Catalyst supports play an important role in providing an electrochemically stable and mechanically robust platform for nanostructured catalyst dispersion, facilitating electron transfer, and accelerating electrocatalytic reactions via the catalyst-support synergistic interaction.[63] A number of carbon materials, such as activated carbon, carbon nanotubes, and graphene have been identified as the state-of-the-art catalyst supports for oxygen redox catalysis.[50,64] 2D graphene is of particular interest as the support to host and grow nanostructured organic/inorganic catalysts due to its ultrahigh specific surface area (≈2630 m^2 g^{-1}) and ability to tune its interactions with precursor species or catalyst materials.[65] Various graphene-supported nanocomposites, such as graphene/carbon nanotubes,[66] graphene/metal oxides,[41,67,68] graphene/transition-metal chalcogenides,[69] and graphene/transition-metal macrocycle complexes[70] have been demonstrated to induce favorable catalyst-support interactions to provide both activity and stability improvement of catalysts. Lee el al. prepared ionic-liquid (IL)-functionalized graphene, upon which Mn_3O_4 nanoparticles were immobilized.[67] The use of IL-modified graphene as a support improved the stability of Mn_3O_4 nanoparticles during the electrocatalytic cycles, and furthermore acted as an additional electron source to facilitate electron transfer in the oxygen reduction process. Further catalyst improvement of charge/mass transfer was achieved by creating in-plane mesopores in graphene structures.[31] It is worth noting that carbon-supported catalysts may suffer from relatively low lifetimes due to electrochemical corrosion (oxidation) of the carbon (>0.207 vs RHE), particularly at highly oxidative potentials of OER catalysis.[71,72] This would cause the loss or aggregation of supported catalysts and degrades the air electrode durability and performance.

Given the problematic corrosion issues observed with the carbon supports, recent studies have advanced the knowledge on the adaptation of metal oxides as electrochemically more stable supports. Support metal oxides are classified into two categories including ORR/OER-catalytically active (e.g., Co_3O_4) and inactive (e.g., TiO_2, ZnO) materials.[21,71,73,74] The active supports may be viewed from the point of synergistic effect. For example, chemical deposition of Pd nanoparticle catalysts on 3D ordered mesoporous (3DOM) Co_3O_4 support demonstrated superb activity and stability for electrocatalytic ORR and OER (**Figure 6**a).[71] DFT calculations revealed that as the support, the 3DOM Co_3O_4 lowered the Pd d-band center and increased the electron abundance at the Fermi level, leading to improved overall electrode kinetics and conductivity. When using the Pd@3DOM-Co_3O_4 as the bifunctional air electrode,

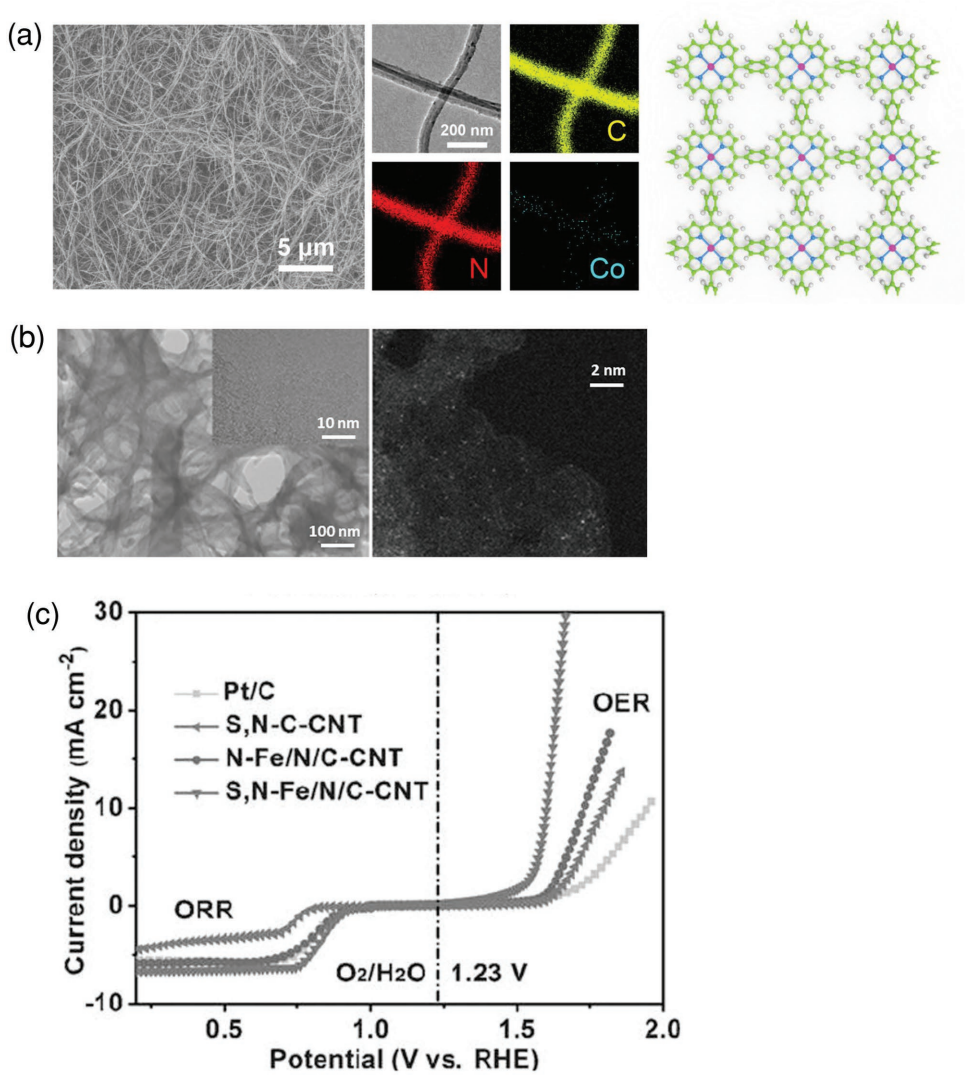

Figure 5. a) SEM image and corresponding EDS elemental mapping of CNT@porphyrin covalent organic framework (POF), as well as chemical structure of the single-layer POF (the hydrogen, carbon, nitrogen, and cobalt atoms are marked with white, green, blue, and pink, respectively). Reproduced with permission.[57] Copyright 2018, Wiley-VCH. b) TEM image (the inset is a high-resolution TEM image showing carbon layers) and HAADF-STEM image of the S,N-Fe/N/C-CNT sample (showing well-dispersed Fe atoms in the carbon layers). Reproduced with permission.[25a] Copyright 2017, Wiley-VCH. c) The overall polarization curves of all samples in the whole ORR and OER region in a 0.1 M KOH solution. Reproduced with permission.[25a] Copyright 2017, Wiley-VCH.

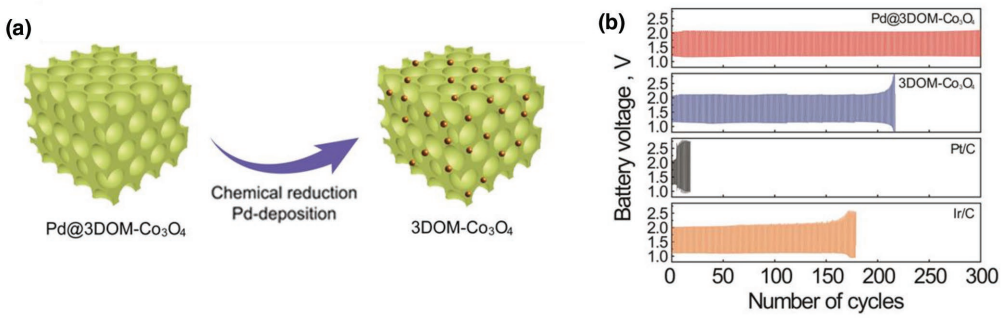

Figure 6. a) Schematic conversion of Pd-deposited 3D ordered mesoporous spinel cobalt oxide (Pd@3DOM-Co_3O_4). b) Charge–discharge cycling performance of the rechargeable zinc–air battery using Pd@3DOM-Co_3O_4, 3DOM-Co_3O_4, Pt/C, and Ir/C obtained with a 10 min cycle period and applied current density of 10 mA cm^{-2}. a) Adapted with permission.[71] Copyright 2018, Elsevier. b) Reproduced with permission.[71] Copyright 2018, Elsevier.

the zinc–air battery stably operated for 300 charge/discharge cycles over a period of 50 h (10 min per a charge/discharge cycle) while effectively retaining its initial performance, which is significantly greater than those of 3DOM-Co_3O_4, Pt/C, and Ir/C (Figure 6b). Moreover, synergistic improvement in stability was achieved due to an increased dissolution potential of Pd nanoparticles on the 3DOM Co_3O_4 surface. On the other hand, researches of inactive metal oxide supports (e.g., TiO_2, Ti_nO_{2n-1}) mainly focused on controlling their morphological aspects (e.g., surface area, pore volume, and pore-size distribution) and surface chemical composition in order to anchor catalysts firmly through strong metal/support interaction and increase the catalytically active site exposure for the oxygen reactions.[63,73] Nevertheless, the electronic conductivity of metal oxide supports is still a critical issue for electrocatalytic applications.[75] Thus, practical catalyst support materials must be designed such that their surfaces inhibit excessive oxidation and/or are concealed by conductive oxide layers.

2.3. Air Electrode Optimization

An ideally constructed air electrode should facilitate electron transport from the current collector to the catalyst layer, and more importantly, provide channels with ideal diffusion/transportation environments for reaction participants to and away from catalytic active sites. Specifically, the electrode environment that supports the ORR should be semihydrophobic to ensure continuous supply of both oxygen and electrolyte access to the catalytically active sites, and the electrode environment supporting the OER should be hydrophilic to prevent oxygen gas bubbles from sticking and blocking the active surface. The amount and distribution of the liquid phase (alkaline electrolyte) within the air electrode has a strong impact on charge/mass transport processes.[76] Compared with hydroxide ion diffusion, oxygen transfer is usually the bottleneck owing to its low solubility in aqueous solutions.[77] Therefore, ensuring continuous and abundant supply of oxygen is of great importance to allow high current densities to be drawn in zinc–air batteries. Typically hydrophobic polymer binders (e.g., Nafion and polytetrafluoroethylene) are used in the fabrication of air electrode to attain an appropriate hydrophobic/hydrophilic balance for the surrounding bifunctional catalysts, but their electrochemical and mechanical stability were called into question during cell operations.[78] Current researches on binder-free air electrodes that are directly integrated with bifunctional oxygen catalysts are motivated by the above challenge.[79] To this end, binder-free bifunctional air electrodes having catalysts, with various compositions and hierarchical porous structures, directly grown on conductive current collectors have been vigorously studied and exhibited significantly improved stability and reduced voltage losses in zinc–air batteries.[78c,80,81] For example, a characteristic binder-free bifunctional air electrode was prepared by the direct growth of mesoporous Co_3O_4 nanowire arrays on a stainless steel mesh as a conductive current collector.[82] This integrative design can enhance the electron transfer between catalytic layer and current collector, thus improving voltage efficiency for both ORR and OER. In an attempt to maximize the utilization of current collectors, Xu et al. developed a cross-stacked and porous carbon-nanotube sheet that severed as a gas diffusion layer, a catalyst layer and a current collector.[83] The battery employing such integrated air electrode exhibited enhanced discharge/charge rate performance. However, the oxygen transport paths in these binder-free bifunctional air electrodes were generally limited by flooded pores, which cut off the oxygen supply between electrode and surrounding environment.[84] A general strategy is to employ a hydrophobic gas diffusion layer as the backing layer,[81] which inevitably scarifies the gravimetric and volumetric energy density of the battery, therefore call for better integrative air electrode architecture with enhanced diffusion of oxygen to the reaction zone. Visual (e.g., X-ray tomography and magnetic resonance imaging) and quantitative understanding of underlying transport processes in these electrodes during the battery operation is necessary so as to circumvent oxygen diffusion barriers.[77,85]

3. Noteworthy Concepts

On top of the existing zinc–air batteries optimization strategies focused on engineering of bifunctional oxygen electrocatalysts, numerous interesting design ideas have also been proposed in recent years. These novel strategies includes the hybrid cathode/air electrode that demonstrated improved battery voltage and power density; the photoassisted bifunctional catalysts which utilized light radiation to improve round trip energy efficiency; the aluminum-doped zinc layered double oxides/hydroxides, which outperforms 3D porous Zn/ZnO anode, and molten salt electrolyte which allows for high rate capability and long cycle lifes. It is not possible to discuss them all here; rather we highlight a few novel and promising concepts.

3.1. High-Voltage Hybrid Air Electrode

Theoretically, the highest potential zinc–air batteries can achieved is limited by the oxygen redox reaction. Recently, gains in voltage and energy density have been reported through adaptation of advance catalysts which provide extra energy density by serving as additional cathode active material. These materials would first undergo their reduction/oxidation reaction and then serve as catalyst for ORR/OER. These types of batteries have been referred to as hybrid zinc batteries due to their utilization of both chemistries. The feasibility of the concept was first showcased by Lee and co-worker, whom demonstrated a hybrid zinc batteries design with $NiO/Ni(OH)_2$ composite nanoflakes cathode that achieved energy density of 980W h kg^{-1} (based on active material mass).[86] The adaptation of the $NiO/Ni(OH)_2$ not only generated an extended discharge platform at 1.7 V, their fast kinetics also enables the batteries to achieve high power density of 1000 W kg^{-1} and 5400 W L^{-1} at 25 mA cm^{-1}. Following the initial demonstration, other advance designs such as Co_3O_4 nanosheets on carbon cloth,[87] $NiCo_2O_4$ on carbon coated nickel foam[88] and spinel $MnCo_2O_4$ nanoparticles on nitrogen-doped reduced graphene oxide[89] have also been reported to achieve rechargeable energy densities of 550–850 W h kg^{-1} which can be maintained for hundreds of cycles. Overall, the advantages of these zinc hybrid batteries in

voltage and energy density are clear, but further elongation of their life span at deep cycling will be required, as their cathode materials do eventually suffer capacity fade caused by formation of electrochemically passive species.

3.2. Photoassisted Air Electrode

The combination of photovoltaic cell with electrocatalyst to improve battery round trip efficiency is a known strategy that has been demonstrated in water oxidation and Li–air batteries.[90] The idea is to supply the electrocatalysts with additional charge carriers generated by radiation captured in a p–n junction to reduce the reaction overpotential and thus increase energy efficiency of a system. Recently, the concept is successfully incorporated into zinc–air batteries by Lv et al., who coupled $N_{12}P_5$ with NCNTs to form a photoresponsive bifunctional air electrode. The $N_{12}P_5$ were assigned as the p-type semiconductor and the OER catalyst, while the NCNT would serve the functionality of the n-type material and ORR catalyst.[91] The electrocatalytic performance of the $Ni_{12}P_5$@NCNT hybrid was shown to react positively with light radiation, as examples, their ORR limiting current increased from 4.06 to 4.37 mA cm^{-2} and their bifunctional activities changed from 0.82 to 0.80 V. Similar trends can be observed when they are employed into zinc–air batteries, as the battery overpotential decreased from 0.75 to 0.68 V and round-trip efficiency increased from 61.3% to 64.2% upon light radiation. The overall electrochemical performance of the catalyst may not be comparable to the best performing bifunctional catalysts in recent publications, but it provides new insight into further improvement of the zinc–air battery system.

3.3. Zn–Al Layered-Double-Oxide Anode

Aside from the anode electrode optimization strategies previously discussed, explorations for alternate anodic materials with modified chemistry have also been reported. Among them, 2D nanoflake structured Zn–Al layered double oxides/hydroxides (Zn–Al LDO/LDH) with similar redox potential as Zn/ZnO have recently emerged as promising candidates. Typically, the LDHs can be cycled at modest capacities of 300–400 Ah kg^{-1} for 200–800 cycles, but suffer from low conductivity.[11,92,93] These performance parameters can be further improved by calcination to remove excess hydroxides and carbonates. The resulting LDOs, composed of crystalline ZnO embedded in an amorphous matrix of aluminum-doped zinc oxide, surpass their precursor and achieved reversible capacities around 400–500 Ah kg^{-1} and cycle life between 500 and 1000 cycles.[94,95] The much improved stability of these materials in comparison to Zn/ZnO has been attributed to their layered structure and even current density distribution,[92,94] but bonding between the Zn and Al likely played an important role as well. Currently, reaction mechanism and optimal synthetic/cycling condition of LDOs/LDHs are still under investigation, and the materials have only been employed in alkaline Zn–Ni batteries. However, given the similarities of the anodic chemistry in both systems, incorporation and further optimization of these electrode materials for zinc–air battery systems should be plausible and promising.

3.4. Molten Salt Electrolyte

The room-temperature aqueous alkaline solutions are by far the most commonly adapted electrolytes in the development of zinc–air batteries, because the oxygen redox can be carried out with nonprecious metal catalysts. Unfortunately, the aqueous and alkalinity nature of this electrolyte leads to problems of drying-out and insoluble carbonate precipitation, as well as promoting zinc-dendrite growth and hydrogen evolution, all of them limiting the performance of zinc–air batteries. To this end, a few recent studies have begun to examine high-temperature zinc molten air systems based on molten carbonate eutectic electrolytes.[96,97] For example, a molten electrolyte consisting of $Li_{0.87}Na_{0.63}K_{0.50}CO_3$ eutectic with KOH at 550 °C has been demonstrated to achieve very stable cycling ability, performing 150 charge–discharge cycles with a coulombic efficiency of 94% and an average discharge voltage of ≈1.08 V. Moreover, a high rate capability was achieved at 7.3C while maintaining a coulombic efficiency of over 90%.[97] Although operating at a high temperature and sacrificing some gravimetric performance (additional cell weight for thermal insulation), the molten salt electrolytes offer advantages over their aqueous counterparts, avoiding well-known issues of electrolyte evaporation, carbonate precipitation, zinc-dendrite formation, and hydrogen evolution, which have been plaguing the life span of aqueous zinc–air batteries. More importantly, with high temperature, precious metal catalysts can be replaced by iron- or nickel-based air electrodes for both oxygen reduction/evolution processes. Nevertheless, molten salt electrolytes allowing lower operating temperatures are preferable to suppress corrosion of the air electrode and improve cell cycle life.

4. Conclusion

The excellent theoretical specific energy and volumetric energy density, as well as inherent safety and cost merits of rechargeable zinc–air batteries have promised a particularly exciting future for their applications in EV technologies. Although zinc–air batteries research have made significant progress in the past ten years, we must recognize that many problems remain to be solved for them to become a leading battery technology in EVs. Issues related to low energy efficiency (e.g., 40–70%) and short cycle life (e.g., 100–150 cycles) of zinc–air batteries need to be fundamentally resolved. Keys to success in efficient and long-term battery operation are the zinc and bifunctional air electrodes reversibility and stability. In this review, we have addressed recent achievements and optimisms on both ends of the battery that are considered to be promising in this direction. In case of the zinc electrode, improvements in inhibiting zinc-dendrite formation and capacity loss upon repeated charge–discharge cycles were made by establishment of conductive porous network that ensure even current density distribution or adaption of alternate zinc based active materials. For bifunctional oxygen catalysts, potentially low-cost transition metal oxides and carbon-based materials are good candidates in reducing charge–discharge voltage polarization of the battery. Although ingenious efforts to engineer these catalysts materials have progressed rapidly and shown promising performance

improvement, in-depth understanding of the catalyst working state and the associated reaction mechanisms is important for the design of near-ideal bifunctional catalysts that would substantially increase the efficiency of rechargeable zinc–air batteries. Accordingly, rational structure catalyst designs around known active materials, instead of trial-and-error design strategies, will be necessary such that precise engineering of individual active sites can be achieved. In this regard, single-atom catalysts for bifunctional catalysis could offer good opportunity to identify and control the active sites of interest, which urge further exploration.

Acknowledgements

The authors wish to acknowledge the support provided by the Natural Sciences and Engineering Research Council of Canada (NSERC), Mitacs Accelerate program, the 111 Project (Grant No. D17007), and Henan Center for Outstanding Overseas Scientists (Grant No. GZS2018003).

Conflict of Interest

The authors declare no conflict of interest.

Keywords

bifunctional air electrodes, bifunctional oxygen catalysts, rechargeable zinc–air batteries, reversible zinc electrodes

Received: August 10, 2018
Revised: September 7, 2018
Published online:

[1] a) A. Hodge, B. Crowley, H. Bairstrow, S. Ljubisavljevic, C. Hamilton, P. Morton, D. Kejriwal, C. May, P. Diyachikina, F. South, D. Thong, T. Katayama, A. Park, S. Shin, J. Lewis, Z. Lin, Global Lithium Report, https://newagemetals.com/wp-content/uploads/Macquarie-GlobalLithiumReport310516e245188.pdf (accessed: July 2018); b) J. W. Choi, D. Aurbach, *Nat. Rev. Mater.* **2016**, *1*, 16013; c) A. Mauger, C. Julien, *Ionics* **2017**, *23*, 1933.
[2] Z. P. Cano, D. Banham, S. Ye, A. Hintennach, J. Lu, M. Fowler, Z. Chen, *Nat. Energy* **2018**, *3*, 279.
[3] F. Jing, C. Z. Paul, P. M. Gyu, Y. Aiping, F. Michael, C. Zhongwei, *Adv. Mater.* **2017**, *29*, 1604685.
[4] Natural Resources Canada, Zinc Facts, http://www.nrcan.gc.ca/mining-materials/facts/zinc/2053 (accessed: July 2018).
[5] EOS Energy Storage, https://eosenergystorage.com/#welcome (accessed: July 2018).
[6] a) FluidicEnergy, http://fluidicenergy.com/ (accessed: July 2018); b) ZINCNYX Energy Solutions Inc., http://www.zincnyx.com (accessed: July 2018).
[7] B. Nykvist, M. Nilsson, *Nat. Clim. Change* **2015**, *5*, 329.
[8] a) Y. Li, J. Lu, *ACS Energy Lett.* **2017**, *2*, 1370; b) Y. Li, H. Dai, *Chem. Soc. Rev.* **2014**, *43*, 5257.
[9] J. Fu, Z. P. Cano, M. G. Park, A. Yu, M. Fowler, Z. Chen, *Adv. Mater.* **2017**, *29*, 1604685.
[10] A. R. Mainar, L. C. Colmenares, J. A. Blázquez, I. Urdampilleta, *Int. J. Energy Res.* **2018**, *42*, 903.
[11] S. B. Lai, M. I. Jamesh, X. C. Wu, Y. L. Dong, J. H. Wang, M. Gao, J. F. Liu, X. M. Sun, *Rare Met.* **2017**, *36*, 381.
[12] J. F. Parker, C. N. Chervin, E. S. Nelson, D. R. Rolison, J. W. Long, *Energy Environ. Sci.* **2014**, *7*, 1117.
[13] J. F. Parker, C. N. Chervin, I. R. Pala, M. Machler, M. F. Burz, J. W. Long, D. R. Rolison, *Science* **2017**, *356*, 415.
[14] M. Chamoun, B. J. Hertzberg, T. Gupta, D. Davies, S. Bhadra, B. Van Tassell, C. Erdonmez, D. A. Steingart, *NPG Asia Mater.* **2015**, *7*, e178.
[15] a) Z. Yan, E. Wang, L. Jiang, G. Sun, *RSC Adv.* **2015**, *5*, 83781; b) J. Liu, C. Guan, C. Zhou, Z. Fan, Q. Ke, G. Zhang, C. Liu, J. Wang, *Adv. Mater.* **2016**, *28*, 8732; c) P. Li, Z. Jin, D. Xiao, *Energy Storage Mater.* **2018**, *12*, 232.
[16] a) H. Liu, Y. Zhang, R. Li, X. Sun, S. Désilets, H. Abou-Rachid, M. Jaidann, L. S. Lussier, *Carbon* **2010**, *48*, 1498; b) M. Li, J. Meng, Q. Li, M. Huang, X. Liu, K. A. Owusu, Z. Liu, L. Mai, *Adv. Funct. Mater.* **2018**, *28*, 1802016.
[17] S. Higashi, S. W. Lee, J. S. Lee, K. Takechi, Y. Cui, *Nat. Commun.* **2016**, *7*, 11801.
[18] a) G. Garcia, E. Ventosa, W. Schuhmann, *ACS Appl. Mater. Interfaces* **2017**, *9*, 18691; b) K. Wang, P. Pei, Z. Ma, H. Chen, H. Xu, D. Chen, X. Wang, *J. Mater. Chem. A* **2015**, *3*, 22648.
[19] H. Pan, Y. Shao, P. Yan, Y. Cheng, K. S. Han, Z. Nie, C. Wang, J. Yang, X. Li, P. Bhattacharya, *Nat. Energy* **2016**, *1*, 16039.
[20] a) D. Kundu, B. D. Adams, V. Duffort, S. H. Vajargah, L. F. Nazar, *Nat. Energy* **2016**, *1*, 16119; b) Q. Zhao, W. Huang, Z. Luo, L. Liu, Y. Lu, Y. Li, L. Li, J. Hu, H. Ma, J. Chen, *Sci. Adv.* **2018**, *4*, eaao1761.
[21] T. Ling, D. Y. Yan, Y. Jiao, H. Wang, Y. Zheng, X. Zheng, J. Mao, X. W. Du, Z. Hu, M. Jaroniec, S. Z. Qiao, *Nat. Commun.* **2016**, *7*, 12876.
[22] J. Zhang, Z. Zhao, Z. Xia, L. Dai, *Nat. Nanotechnol.* **2015**, *10*, 444.
[23] a) S. H. Ahn, X. Yu, A. Manthiram, *Adv. Mater.* **2017**, *29*, 1606534; b) Y. Lee, J. Suntivich, K. J. May, E. E. Perry, S. Yang, *J. Phys. Chem. Lett.* **2012**, *3*, 399.
[24] a) J. S. Kim, B. Kim, H. Kim, K. Kang, *Adv. Energy Mater.* **2018**, *8*, 1702774; b) J. Deng, D. Deng, X. Bao, *Adv. Mater.* **2017**, *29*, 1606967.
[25] a) P. Chen, T. Zhou, L. Xing, K. Xu, Y. Tong, H. Xie, L. Zhang, W. Yan, W. Chu, C. Wu, *Angew. Chem., Int. Ed.* **2017**, *56*, 610; b) M. G. Park, D. U. Lee, M. H. Seo, Z. P. Cano, Z. Chen, *Small* **2016**, *12*, 2707; c) Y. Jiang, Y. P. Deng, J. Fu, D. U. Lee, R. Liang, Z. P. Cano, Y. Liu, Z. Bai, S. Hwang, L. Yang, *Adv. Energy Mater.* **2018**, *8*, 1870068.
[26] A. Aijaz, J. Masa, C. Rösler, W. Xia, P. Weide, A. J. Botz, R. A. Fischer, W. Schuhmann, M. Muhler, *Angew. Chem., Int. Ed.* **2016**, *55*, 4087.
[27] a) Y. Liu, C. Xiao, M. Lyu, Y. Lin, W. Cai, P. Huang, W. Tong, Y. Zou, Y. Xie, *Angew. Chem.* **2015**, *127*, 11383; b) O. Mabayoje, A. Shoola, B. R. Wygant, C. B. Mullins, *ACS Energy Lett.* **2016**, *1*, 195; c) H. F. Wang, C. Tang, B. Wang, B. Q. Li, Q. Zhang, *Adv. Mater.* **2017**, *29*, 1702327.
[28] J. P. Collman, P. Denisevich, Y. Konai, M. Marrocco, C. Koval, F. C. Anson, *J. Am. Chem. Soc.* **1980**, *102*, 6027.
[29] J. Sun, H. Yin, P. Liu, Y. Wang, X. Yao, Z. Tang, H. Zhao, *Chem. Sci.* **2016**, *7*, 5640.
[30] a) K. Sakaushi, T. P. Fellinger, M. Antonietti, *ChemSusChem* **2015**, *8*, 1156; b) H. B. Yang, J. Miao, S. F. Hung, J. Chen, H. B. Tao, X. Wang, L. Zhang, R. Chen, J. Gao, H. M. Chen, *Sci. Adv.* **2016**, *2*, e1501122.
[31] J. Fu, F. M. Hassan, C. Zhong, J. Lu, H. Liu, A. Yu, Z. Chen, *Adv. Mater.* **2017**, *29*, 1702526.
[32] a) W. Liu, J. Zhang, Z. Bai, G. Jiang, M. Li, K. Feng, L. Yang, Y. Ding, T. Yu, Z. Chen, *Adv. Funct. Mater.* **2018**, *28*, 1706675; b) S. Mao, Z. Wen, T. Huang, Y. Hou, J. Chen, *Energy Environ. Sci.* **2014**, *7*, 609; c) P. Ganesan, M. Prabu, J. Sanetuntikul, S. Shanmugam, *ACS Catal.* **2015**, *5*, 3625; d) D. U. Lee, M. G. Park, Z. P. Cano, W. Ahn, Z. Chen, *ChemSusChem* **2018**, *11*, 406.
[33] D. U. Lee, P. Xu, Z. P. Cano, A. G. Kashkooli, M. G. Park, Z. Chen, *J. Mater. Chem. A* **2016**, *4*, 7107.

[34] Z. W. Seh, J. Kibsgaard, C. F. Dickens, I. Chorkendorff, J. K. Nørskov, T. F. Jaramillo, *Science* **2017**, *355*, eaad4998.
[35] Y. Meng, W. Song, H. Huang, Z. Ren, S. Y. Chen, S. L. Suib, *J. Am. Chem. Soc.* **2014**, *136*, 11452.
[36] a) Y. Li, M. Gong, Y. Liang, J. Feng, J. E. Kim, H. Wang, G. Hong, B. Zhang, H. Dai, *Nat. Commun.* **2013**, *4*, 1805; b) J. Pan, Y. Y. Xu, H. Yang, Z. Dong, H. Liu, B. Y. Xia, *Adv. Sci.* **2018**, *5*, 1700691.
[37] a) J. S. Lee, S. T. Kim, R. Cao, N. S. Choi, M. Liu, K. T. Lee, J. Cho, *Adv. Energy Mater.* **2011**, *1*, 34; b) E. Davari, D. G. Ivey, *Sustainable Energy Fuels* **2018**, *2*, 39; c) Z. F. Huang, J. Wang, Y. Peng, C.-Y. Jung, A. Fisher, X. Wang, *Adv. Energy Mater.* **2017**, *7*, 1700544.
[38] Z. Chen, A. Yu, D. Higgins, H. Li, H. Wang, Z. Chen, *Nano Lett.* **2012**, *12*, 1946.
[39] a) H. W. Park, D. U. Lee, P. Zamani, M. H. Seo, L. F. Nazar, Z. Chen, *Nano Energy* **2014**, *10*, 192; b) G. Li, X. Wang, J. Fu, J. Li, M. G. Park, Y. Zhang, G. Lui, Z. Chen, *Angew. Chem., Int. Ed.* **2016**, *55*, 4977; c) S. K. Singh, V. M. Dhavale, S. Kurungot, *ACS Appl. Mater. Interfaces* **2015**, *7*, 21138.
[40] a) J. Liang, R. F. Zhou, X. M. Chen, Y. H. Tang, S. Z. Qiao, *Adv. Mater.* **2014**, *26*, 6074; b) Y. Zhang, B. Ouyang, J. Xu, G. Jia, S. Chen, R. S. Rawat, H. J. Fan, *Angew. Chem., Int. Ed.* **2016**, *55*, 8670; c) L. Lin, Q. Zhu, A. W. Xu, *J. Am. Chem. Soc.* **2014**, *136*, 11027.
[41] Y. Liang, Y. Li, H. Wang, J. Zhou, J. Wang, T. Regier, H. Dai, *Nat. Mater.* **2011**, *10*, 780.
[42] A. P. Tiwari, D. Kim, Y. Kim, H. Lee, *Adv. Energy Mater.* **2017**, *7*, 1602217.
[43] a) S. Jin, M. J. Kevin, G. A. Hubert, G. B. John, S. H. Yang, *Science* **2011**, *334*, 1383; b) S. Gupta, W. Kellogg, H. Xu, X. Liu, J. Cho, G. Wang, *Chem. - Asian J.* **2016**, *11*, 10.
[44] a) L. Xu, Q. Jiang, Z. Xiao, X. Li, J. Huo, S. Wang, L. Dai, *Angew. Chem., Int. Ed.* **2016**, *55*, 5277; b) F. Cheng, T. Zhang, Y. Zhang, J. Du, X. Han, J. Chen, *Angew. Chem.* **2013**, *125*, 2534.
[45] a) J. Jung, H. Y. Jeong, J. S. Lee, M. G. Kim, J. Cho, *Angew. Chem.* **2014**, *126*, 4670; b) C. F. Chen, G. King, R. M. Dickerson, P. A. Papin, S. Gupta, W. R. Kellogg, G. Wu, *Nano Energy* **2015**, *13*, 423.
[46] a) J. Bao, X. Zhang, B. Fan, J. Zhang, M. Zhou, W. Yang, X. Hu, H. Wang, B. Pan, Y. Xie, *Angew. Chem.* **2015**, *127*, 7507; b) X. Fan, M. S. Balogun, Y. Huang, Y. Tong, *ChemElectroChem* **2017**, *4*, 2453; c) X. Lei, J. Qianqian, X. Zhaohui, L. Xingyue, H. Jia, W. Shuangyin, D. Liming, *Angew. Chem., Int. Ed.* **2016**, *55*, 5277.
[47] N. Kim, Y. J. Sa, T. S. Yoo, S. R. Choi, R. A. Afzal, T. Choi, Y. Seo, K. Lee, J. Y. Hwang, W. S. Choi, S. H. Joo, *Sci. Adv.* **2018**, *4*, eaap9360.
[48] Y. Wang, T. Zhou, K. Jiang, P. Da, Z. Peng, J. Tang, B. Kong, W. Cai, Z. Yang, G. Zheng, *Adv. Energy Mater.* **2014**, *4*, 1400696.
[49] X. Liu, L. Dai, *Nat. Rev. Mater.* **2016**, *1*, 16064.
[50] H. Zhang, R. Lv, *J. Materiomics* **2018**, *4*, 95.
[51] a) H. B. Yang, J. Miao, S. F. Hung, J. Chen, H. B. Tao, X. Wang, L. Zhang, R. Chen, J. Gao, H. M. Chen, L. Dai, B. Liu, *Sci. Adv.* **2016**, *2*, e1501122; b) K. Gong, F. Du, Z. Xia, M. Durstock, L. Dai, *Science* **2009**, *323*, 760.
[52] Z. Yao, J. Yan, G. Lei, J. Mietek, Q. S. Zhang, *Angew. Chem., Int. Ed.* **2013**, *52*, 3110.
[53] a) K. Qu, Y. Zheng, S. Dai, S. Z. Qiao, *Nano Energy* **2016**, *19*, 373; b) X. Zheng, X. Cao, J. Wu, J. Tian, C. Jin, R. Yang, *Carbon* **2016**, *107*, 907; c) W. Schöfberger, F. Faschinger, S. Chattopadhyay, S. Bhakta, B. Mondal, J. A. Elemans, S. Müllegger, S. Tebi, R. Koch, F. Klappenberger, *Angew. Chem., Int. Ed.* **2016**, *55*, 2350; d) W. Zhang, W. Lai, R. Cao, *Chem. Rev.* **2017**, *117*, 3717.
[54] J. Hao, W. Yang, Z. Peng, C. Zhang, Z. Huang, W. Shi, *ACS Catal.* **2017**, *7*, 4214.
[55] L. Guo, J. Deng, G. Wang, Y. Hao, K. Bi, X. Wang, Y. Yang, *Adv. Funct. Mater.* **2018**, *28*, 1804540.
[56] a) F. Zhang, Y. Ge, H. Chu, P. Dong, R. Baines, Y. Pei, M. Ye, J. Shen, *ACS Appl. Mater. Interfaces* **2018**, *10*, 7087; b) H. Zhang, T. Wang, A. Sumboja, W. Zang, J. Xie, D. Gao, S. J. Pennycook, Z. Liu, C. Guan, J. Wang, *Adv. Funct. Mater.* **2018**, *28*, 1804846.
[57] B. Q. Li, S. Y. Zhang, B. Wang, Z. J. Xia, C. Tang, Q. Zhang, *Energy Environ. Sci.* **2018**, *11*, 1723.
[58] a) Y. J. Sa, D. J. Seo, J. Woo, J. T. Lim, J. Y. Cheon, S. Y. Yang, J. M. Lee, D. Kang, T. J. Shin, H. S. Shin, *J. Am. Chem. Soc.* **2016**, *138*, 15046; b) Z. Hu, Z. Zhang, Z. Li, M. Dou, F. Wang, *ACS Appl. Mater. Interfaces* **2017**, *9*, 16109.
[59] a) Y. Zhen, C. Wang, Z. Wu, Y. Xiong, Q. Xu, S. Yu, H. Jiang, *Adv. Mater.* **2015**, *27*, 5010; b) L. Ma, S. Chen, Z. Pei, Y. Huang, G. Liang, F. Mo, Q. Yang, J. Su, Y. Gao, J. A. Zapien, C. Zhi, *ACS Nano* **2018**, *12*, 1949.
[60] P. Chen, T. Zhou, L. Xing, K. Xu, Y. Tong, H. Xie, L. Zhang, W. Yan, W. Chu, C. Wu, Y. Xie, *Angew. Chem., Int. Ed.* **2017**, *56*, 610.
[61] J. Wei, Y. Liang, Y. Hu, B. Kong, J. Zhang, Q. Gu, Y. Tong, X. Wang, S. P. Jiang, H. Wang, *Angew. Chem., Int. Ed.* **2016**, *55*, 12470.
[62] a) L. Yang, D. Cheng, H. Xu, X. Zeng, X. Wan, J. Shui, Z. Xiang, D. Cao, *Proc. Natl. Acad. Sci. USA* **2018**, *115*, 6626; b) Y. Zheng, Y. Jiao, Y. Zhu, Q. Cai, A. Vasileff, L. H. Li, Y. Han, Y. Chen, S. Z. Qiao, *J. Am. Chem. Soc.* **2017**, *139*, 3336.
[63] J. Masa, W. Xia, I. Sinev, A. Zhao, Z. Sun, S. Grützke, P. Weide, M. Muhler, W. Schuhmann, *Angew. Chem., Int. Ed.* **2014**, *53*, 8508.
[64] J. Liang, S. Z. Qiao, G. Q. Lu, D. Hulicova-Jurcakova, in *Novel Carbon Adsorbents* (Ed: J. M. D. Tascón), Elsevier, Oxford **2012**, p. 549.
[65] L. Ji, P. Meduri, V. Agubra, X. Xiao, M. Alcoutlabi, *Adv. Energy Mater.* **2016**, *6*, 1502159.
[66] a) G. L. Tian, M. Q. Zhao, D. Yu, X. Y. Kong, J. Q. Huang, Q. Zhang, F. Wei, *Small* **2014**, *10*, 2251; b) R. Li, Z. Wei, X. Gou, *ACS Catal.* **2015**, *5*, 4133.
[67] J. S. Lee, T. Lee, H. K. Song, J. Cho, B. S. Kim, *Energy Environ. Sci.* **2011**, *4*, 4148.
[68] L. Wei, H. E. Karahan, S. Zhai, H. Liu, X. Chen, Z. Zhou, Y. Lei, Z. Liu, Y. Chen, *Adv. Mater.* **2017**, *29*, 1701410;
[69] a) Q. Liu, J. Jin, J. Zhang, *ACS Appl. Mater. Interfaces* **2013**, *5*, 5002; b) S. Dou, L. Tao, J. Huo, S. Wang, L. Dai, *Energy Environ. Sci.* **2016**, *9*, 1320.
[70] a) C. Tang, B. Wang, H. F. Wang, Q. Zhang, *Adv. Mater.* **2017**, *29*, 1703185; b) I. Kruusenberg, J. Mondal, L. Matisen, V. Sammelselg, K. Tammeveski, *Electrochem. Commun.* **2013**, *33*, 18; c) D. M. Morales, J. Masa, C. Andronescu, Y. U. Kayran, Z. Sun, W. Schuhmann, *Electrochim. Acta* **2016**, *222*, 1191.
[71] M. H. Seo, M. G. Park, D. U. Lee, X. Wang, W. Ahn, S. H. Noh, S. M. Choi, Z. P. Cano, B. Han, Z. Chen, *Appl. Catal., B* **2018**, *239*, 677.
[72] G. Fu, Y. Tang, J. Lee, *ChemElectroChem* **2018**, *5*, 1424.
[73] a) C. Alegre, E. Modica, C. Lo Vecchio, S. Siracusano, A. S. Aricò, V. Baglio, *Int. J. Hydrogen Energy* **2016**, *41*, 19579; b) S. Y. Huang, P. Ganesan, W. S. Jung, N. Cadirov, B. N. Popov, *ECS Trans.* **2010**, *33*, 1979.
[74] Y. Cheng, S. Dou, J. P. Veder, S. Wang, M. Saunders, S. P. Jiang, *ACS Appl. Mater. Interfaces* **2017**, *9*, 8121.
[75] S. M. Kim, H. Lee, J. Y. Park, *Catal. Lett.* **2015**, *145*, 299.
[76] Z. Lu, W. Xu, J. Ma, Y. Li, X. Sun, L. Jiang, *Adv. Mater.* **2016**, *28*, 7155.
[77] D. Schröder, T. Arlt, U. Krewer, I. Manke, *Electrochem. Commun.* **2014**, *40*, 88.
[78] a) S. Holdcroft, *Chem. Mater.* **2014**, *26*, 381; b) B. Li, X. Ge, F. T. Goh, T. A. Hor, D. Geng, G. Du, Z. Liu, J. Zhang, X. Liu, Y. Zong, *Nanoscale* **2015**, *7*, 1830; c) Q. Liu, Y. Wang, L. Dai, J. Yao, *Adv. Mater.* **2016**, *28*, 3000.
[79] a) X. Cai, L. Lai, J. Lin, Z. Shen, *Mater. Horiz.* **2017**, *4*, 945; b) P. Jing, X. Y. Yang, Y. Huan, D. Zehua, L. Hongfang, X. B. Yu, *Adv. Sci.* **2018**, *5*, 1700691.
[80] T. Y. Ma, J. Ran, S. Dai, M. Jaroniec, S. Z. Qiao, *Angew. Chem., Int. Ed.* **2015**, *54*, 4646.

[81] J. Fu, F. M. Hassan, J. Li, D. U. Lee, A. R. Ghannoum, G. Liu, M. A. Hoque, Z. Chen, *Adv. Mater.* **2016**, *28*, 6421.
[82] D. U. Lee, J. Y. Choi, K. Feng, H. W. Park, Z. Chen, *Adv. Energy Mater.* **2014**, *4*, 1301389.
[83] Y. Xu, Y. Zhang, Z. Guo, J. Ren, Y. Wang, H. Peng, *Angew. Chem., Int. Ed.* **2015**, *54*, 15390.
[84] K. Xu, A. Loh, B. Wang, X. Li, *J. Electrochem. Soc.* **2018**, *165*, A809.
[85] a) R. F. Lang, T. Arlt, I. Manke, J. Kowal, *J. Power Sources* **2017**, *370*, 45; b) D. Schröder, C. L. Bender, T. Arlt, M. Osenberg, A. Hilger, S. Risse, M. Ballauff, I. Manke, J. Janek, *J. Phys. D: Appl. Phys.* **2016**, *49*, 404001; c) M. M. Britton, P. M. Bayley, P. C. Howlett, A. J. Davenport, M. Forsyth, *J. Phys. Chem. Lett.* **2013**, *4*, 3019.
[86] D. U. Lee, J. Fu, M. G. Park, H. Liu, A. Ghorbani Kashkooli, Z. Chen, *Nano Lett.* **2016**, *16*, 1794.
[87] P. Tan, B. Chen, H. Xu, W. Cai, W. He, M. Liu, Z. Shao, M. Ni, *Small* **2018**, *14*, 1800225.
[88] B. Li, J. Quan, A. Loh, J. Chai, Y. Chen, C. Tan, X. Ge, T. S. A. Hor, Z. Liu, H. Zhang, Y. Zong, *Nano Lett.*. **2017**, *17*, 156.
[89] A. Qaseem, F. Chen, C. Qiu, A. Mahmoudi, X. Wu, X. Wang, R. L. Johnston, *Part. Part. Syst. Charact.* **2017**, *34*, 1700097.
[90] a) M. Yu, X. Ren, L. Ma, Y. Wu, *Nat. Commun.* **2014**, *5*, 5111; b) S. Y. Reece, J. A. Hamel, K. Sung, T. D. Jarvi, A. J. Esswein, J. J. Pijpers, D. G. Nocera, *Science* **2011**, *334*, 645.
[91] J. Lv, S. C. Abbas, Y. Huang, Q. Liu, M. Wu, Y. Wang, L. Dai, *Nano Energy* **2018**, *43*, 130.
[92] X. Fan, Z. Yang, R. Wen, B. Yang, W. Long, *J. Power Sources* **2013**, *224*, 80.
[93] R. Wang, Z. Yang, B. Yang, T. Wang, Z. Chu, *J. Power Sources* **2014**, *251*, 344.
[94] a) J. Huang, Z. Yang, R. Wang, Z. Zhang, Z. Feng, X. Xie, *J. Mater. Chem. A* **2015**, *3*, 7429; b) Y. Liu, Z. Yang, X. Xie, J. Huang, X. Wen, *Electrochim. Acta* **2015**, *185*, 190.
[95] J. Long, Z. Yang, X. Zeng, J. Huang, *RSC Adv.* **2016**, *6*, 92896.
[96] a) S. Liu, W. Han, B. Cui, X. Liu, F. Zhao, J. Stuart, S. Licht, *J. Power Sources* **2017**, *342*, 435; b) S. Licht, B. Cui, J. Stuart, B. Wang, J. Lau, *Energy Environ. Sci.* **2013**, *6*, 3646.
[97] S. Liu, W. Han, B. Cui, X. Liu, H. Sun, J. Zhang, M. Lefler, S. Licht, *J. Electrochem. Soc.* **2018**, *165*, A149.